frontiers | Frontiers in Materials

ORIGINAL RESEARCH
published: 25 May 2022
doi: 10.3389/fmats.2022.885608

Theoretical Investigation of Effects of Transition Elements on Phase Stabilities and Elastic Properties of the γ′ Phase in Co–V–Ta Superalloys

Youheng Chen[1], *Cuiping Wang*[1,2], *Chi Zhang*[1], *Chen Yang*[1], *Jiajia Han*[1,2]* and *Xingjun Liu*[1,2,3]*

[1]College of Materials and Fujian Provincial Key Laboratory of Materials Genome, Xiamen University, Xiamen, China, [2]Xiamen Key Laboratory of High Performance Metals and Materials, Xiamen University, Xiamen, China, [3]Institute of Materials Genome and Big Data, Harbin Institute of Technology, Shenzhen, China

In order to improve the thermal stability and mechanical properties of W-free light-weight Co–V–Ta-based superalloys, the effects of alloying elements including Sc, Ti, Cr, Mn, Fe, Ni, Y, Zr, Nb, Mo, Tc, Ru, Rh, Pd, Hf, W, Re, Os, Ir, and Pt on γ′-Co_3(V, Ta) stability and elastic properties were studied. The results from the reaction energy indicate that Sc, Ti, Y, Zr, Nb, Mo, Hf, and W tend to occupy the V site, whereas Cr, Mn, Fe, Ni, Tc, Ru, Rh, Pd, Re, Os, Ir, and Pt prefer to occupy the Co site. It was found that Sc, Ti, Y, Zr, Fe, and Mn stabilize the γ′-Co_3(V, Ta) phase by raising the phase-transfer energy. The addition of Mo and W increases the bulk modulus, shear modulus, and Young's modulus. According to Pugh's classical criterion, the γ′-Co_3(V, Ta) phase is an intrinsically brittle material, and the addition of elements such as Tc and Re significantly enhances the ductility. At finite temperature, the doping of Sc, Ti, Mn, Fe, and Hf enhances the relative stability of the γ′-Co_3(V, Ta) phase in the whole temperature range from 0 to 1200 K and are candidates for improving the stability of the γ′-Co_3(V, Ta) phase.

Keywords: first-principle calculations, Co–V–Ta-based superalloys, mechanical properties, thermodynamic properties, phase stability

OPEN ACCESS

Edited by:
Yong A. Zhang,
University of Science and Technology Beijing, China

Reviewed by:
Souraya Goumri-Said,
Alfaisal University, Saudi Arabia
Xiaotian Wang,
Southwest University, China

***Correspondence:**
Jiajia Han
jiajiahan@xmu.edu.cn
Xingjun Liu
xjliu@hit.edu.cn

Specialty section:
This article was submitted to Structural Materials, a section of the journal Frontiers in Materials

Received: *28 February 2022*
Accepted: *21 April 2022*
Published: *25 May 2022*

Citation:
Chen Y, Wang C, Zhang C, Yang C, Han J and Liu X (2022) Theoretical Investigation of Effects of Transition Elements on Phase Stabilities and Elastic Properties of the γ′ Phase in Co–V–Ta Superalloys. Front. Mater. 9:885608. doi: 10.3389/fmats.2022.885608

1 INTRODUCTION

Since the discovery of the γ′ phase in the Co–Al–W ternary system (Sato et al., 2006), extensive attention has been attracted to the γ′-strengthened Co-based superalloys. The coherent γ/γ′ structure makes this new class of Co-based superalloy possess good high temperature strength and creep resistance, and its solidus and liquidus temperatures are 100°C–150°C higher than those of advanced Ni-based alloys (Pollock et al., 2010). Therefore, the development of γ′-strengthened Co-based superalloys has become a significant subject for research. It has been reported that W can effectively stabilize the γ′ phase and elevate the γ′ solvus temperature in Co-based superalloys (Pyczak et al., 2015). However, the heavy element W significantly increases the density of Co–Al–W-based superalloys (Shi et al., 2015), which is unfavorable for industrial applications, such as turbine blades. Recently, a considerable amount of literature work has been focused on the development of W-free Co-based high-temperature superalloys, aiming at reducing the mass density while maintaining the microstructure stability and high-temperature properties (Bantounas et al., 2019; Reyes Tirado et al., 2019; Migas et al., 2020; Reyes Tirado et al., 2020; Ruan et al., 2020;

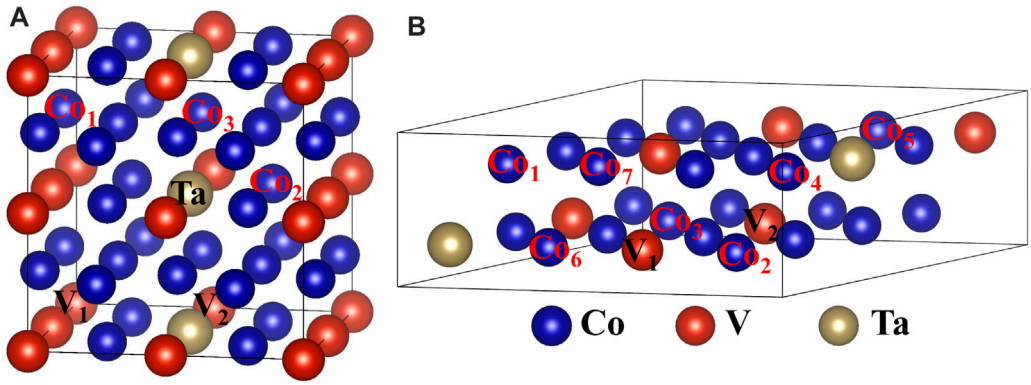

FIGURE 1 | (A) Crystal structure of $L1_2$-ordered Co_3(V, Ta) with six nonequivalent sites (Co_1, Co_2, Co_3, V_1, V_2, and Ta) for the substitution by TM elements. **(B)** Crystal structure of $D0_{19}$-ordered Co_3(V, Ta) with 10 nonequivalent sites (Co_1, Co_2, Co_3, Co_4, Co_5, Co_6, Co_7, V_1, V_2, and Ta) for the substitution by TM elements.

Davydov et al., 2021). Recently, Ruan et al. (2020) used machine learning algorithms and CALPHAD methods to successfully design a Co–V–Ta alloy with a wide γ/γ′ two-phase region, lower density than that of the Co–9Al–9.8W alloy (8.86 vs. 9.82 g/cm^3), and higher yield strength. These advantages make the Co–V–Ta system a promising base alloy for further development.

However, the stability of the γ′ phase in the Co–V–Ta system is relatively low, and the volume fraction of the γ′ phase is not high enough. To improve the γ′ phase stability and volume fraction, an understanding of effects of alloying elements on the γ′ phase stability is required. Ruan et al. (2020) found that Ti effectively increases the γ′ solvus temperature by 70°C. Reyes Tirado et al. (2019) studied the alloying effects of Al, Ti, and Cr additions on the γ/γ′ microstructure and discovered that Al can stabilize the γ′ phase, and the addition of Ti and Ni has no significant effects on γ′ stability. Cr can slightly increase the γ′ volume. However, compared to the commercial Ni-based alloys, which contain upward of ten additional alloying elements, the research studies on alloying effects in the Co–V–Ta system are quite insufficient. The traditional experimental methods are quite expensive and time-consuming. Alternatively, the first-principle method provides an efficient way to explore the alloying effects and can give a deeper insight into the electronical interactions, which is hard to obtain by experiments.

To deeply understand the alloying effects of TM elements (including Sc, Ti, Cr, Mn, Fe, Ni, Y, Zr, Nb, Mo, Tc, Ru, Rh, Pd, Hf, W, Re, Os, Ir, and Pt) on the γ′-Co_3(V, Ta) phase, the first-principle calculations were performed to systematically investigate the phase stabilities and mechanical and thermodynamic properties of alloying effects of TM elements on the γ′-Co_3(V, Ta) phase. First, the site preference of TM elements in the γ′-Co_3(V, Ta) phase was calculated. On this basis, the stability and mechanical properties of γ′-Co_3(V, Ta) were evaluated. Further studies on the electronic structure explain the alloying effects of TM elements. Our research could be highly valuable for the interpretation of the experimental results in the Co-based superalloy, which provides very useful guidelines for the design and preparation of W-free Co–V–Ta-based superalloys.

2 COMPUTATIONAL METHODS

2.1 Structural Model

The γ′-Co_3(V, Ta) phase is built as a 2 × 2 × 2 supercell with Co at the cubic corner sites and V/Ta at the face center sites, as shown in **Figure 1A**. The supercell has 24 Co atoms, six V atoms, and two Ta atoms, which is consistent with experimental results (Ruan et al., 2020). There are six non-equivalent substitutional sites, namely, Co_1, Co_2, Co_3, V_1, V_2, and Ta in **Figure 1A**. Since the $D0_{19}$ phase is preferred in both Co–V and Co–Ta binary systems (Drapier and Coutsouradis, 1968; Wang et al., 2018), it is rational to consider the $D0_{19}$ phase as the main competing phase in the Co–V–Ta ternary system. The $D0_{19}$-Co_3(V, Ta) phase is built as a 2 × 2 × 1 supercell, and 10 non-equivalent substitutional sites, marked as Co_1, Co_2, Co_3, Co_4, Co_5, Co_6, Co_7, V_1, and V_2, Ta are shown in **Figure 1B**.

2.2 Reaction Energy

To reveal the preferred substitutional sites of TM elements, the following reaction process is considered:

$$Co_{24}V_6Ta_2 + X \rightarrow \begin{cases} Co_{23}V_6Ta_2X + Co \\ Co_{24}V_5Ta_2X + V \\ Co_{24}V_6Ta_1X + Ta. \end{cases} \quad (1)$$

The reaction energy is defined as follows:

$$E_{sub}^{X\rightarrow i} = (E_{sub} + E_i) - \left(E_{pure} + E_X\right), \quad (2)$$

where E_{sub} and E_{pure} refer to the total energy of the substituted system and pure system, respectively. E_i/E_X is the energy per atom of Co, V, Ta, and X (X = Sc, Ti, Cr, Mn, Fe, Ni, Y, Zr, Nb, Mo, Tc, Ru, Rh, Pd, Hf, W, Re, Os, Ir, and Pt) in their most stable bulk structure. The preferred substitutional sites are determined by those with the lowest reaction energy $E_{sub}^{X\rightarrow i}$.

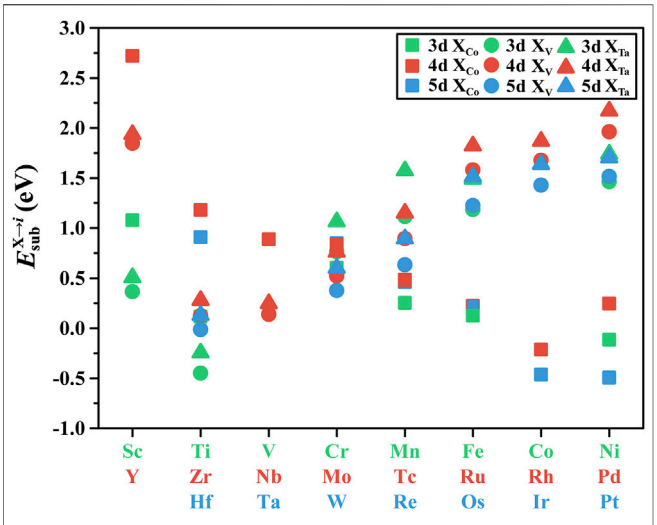

FIGURE 2 | Reaction energy for the TM-substituted γ′-Co_3(V, Ta). The square, round, and triangle markers denote TM elements occupying the Co, V, and Ta sites, respectively.

TABLE 1 | Site preference and formation enthalpies ΔH (eV/atom) of X-substituted γ′-Co_3(V, Ta).

X	ΔH	Site	X	ΔH	Site
Sc	−0.169	V_2	Tc	−0.165	Co_1
Ti	−0.194	V_2	Ru	−0.173	Co_1
Cr	−0.161	Co_2	Rh	−0.187	Co_2
Mn	−0.172	Co_1	Pd	−0.172	Co_2
Fe	−0.176	Co_1	Hf	−0.180	V_2
Ni	−0.183	Co_3	W	−0.168	V_2
Y	−0.122	V_2	Re	−0.165	Co_1
Zr	−0.176	V_2	Os	−0.173	Co_1
Nb	−0.176	V_1	Ir	−0.194	Co_1
Mo	−0.164	V_2	Pt	−0.195	Co_1

2.3 Phase Stability

Once the preferred sites are determined, the phase stability can be decided by its formation enthalpy, ΔH.

$$\Delta H = \left(E_{sub} - \sum_i n_i E_i\right) \Big/ 32, \tag{3}$$

where n_i is the number of i atoms in the phase. A negative formation enthalpy implies the thermal stability at 0 K. Other than ΔH, the stability of the $L1_2$ structure is also related to the formation enthalpy of the competitive phase in the Co-based superalloys. Here, we considered the $D0_{19}$ phase as the competing phase and introduced the phase transfer energy to evaluate the relative stability between $L1_2$ and $D0_{19}$ structures, which is defined as follows:

$$\Delta E(L1_2 \rightarrow D0_{19}) = \Delta H_{D0_{19}} - \Delta H_{L1_2}.$$

2.4 Mechanical Properties

To understand the effects of TM elements on mechanical properties, the elastic constants are calculated using the stress–strain method (Shang et al., 2007). Based on Hooke's law, the relationship between strain and stress is defined as follows:

$$\sigma_i = \sum_j C_{ij}\varepsilon_j, \tag{4}$$

where C_{ij} is the elastic constant.

According to the symmetry of the $L1_2$ structure, only C_{11}, C_{12},, and C_{44} are independent entries. Due to the relatively small size of the supercell, the TM elements may induce local lattice distortion and break the symmetry. As a result, the average C_{ij} was used in this study to ensure the comparability of the results. For the $L1_2$ structure, the results are averaged as follows:

$$\bar{C}_{11} = (C_{11} + C_{22} + C_{33})/3, \quad \bar{S}_{11} = (S_{11} + S_{22} + S_{33})/3, \tag{5}$$

$$\bar{C}_{12} = (C_{12} + C_{13} + C_{23})/3, \quad \bar{S}_{12} = (S_{12} + S_{13} + S_{23})/3, \tag{6}$$

$$\bar{C}_{44} = (C_{44} + C_{55} + C_{66})/3, \quad \bar{S}_{44} = (S_{44} + S_{55} + S_{66})/3, \tag{7}$$

where S_{ij} are elastic compliance constants.

$$[S_{ij}] = [C_{ij}]^{-1}. \tag{8}$$

Based on the calculated results, the aggregate properties can be calculated by

$$B_V = (\bar{C}_{11} + 2\bar{C}_{12})/3, \quad B_R = 1/(3\bar{S}_{11} + 6\bar{S}_{12}), \tag{9}$$

$$G_V = (\bar{C}_{11} - \bar{C}_{12} + 3\bar{C}_{44})/5, \quad G_R = 5/(4\bar{S}_{11} - 4\bar{S}_{12} + 3), \tag{10}$$

$$B_H = (B_V + B_R)/2, \tag{11}$$

$$G_H = (G_V + G_R)/2, \tag{12}$$

$$E_H = (9B_H G_H)/(3B_H + G_H), \tag{13}$$

$$\nu = 3B_H - 2G_H/2(3B_H + G_H), \tag{14}$$

where B, G, and ν denote the bulk, shear, Young's moduli, and Poisson's ratio, respectively.

2.5 Calculation Details

All calculations were performed using the Vienna ab initio simulation package (VASP) (Kresse and Furthmüller, 1996) based on the density functional theory using the projector augmented wave (PAW) pseudopotential method (Kresse and Joubert, 1999). The generalized gradient approximation (GGA) of Perdew–Burke–Ernzerhof (PBE) was used to calculate the exchange–correlation functional. The cut-off energy of the plane-wave basis was set to 450 eV. After careful testing, the Brillouin zone was sampled by 7 × 7 × 7 and 3 × 3 × 7 k-meshes for $L1_2$ and $D0_{19}$ structures using the Monkhort–Pack scheme (Monkhorst and Pack, 1976). In the ionic relaxation, the Methfessel–Paxton method (Methfessel and Paxton, 1989) was used for reciprocal integration, and the smearing width was set to 0.12 eV. The energy and force convergence criteria were 10^{-5} eV/atom and 10^{-2} eV/Å, respectively. Spin polarization was considered.

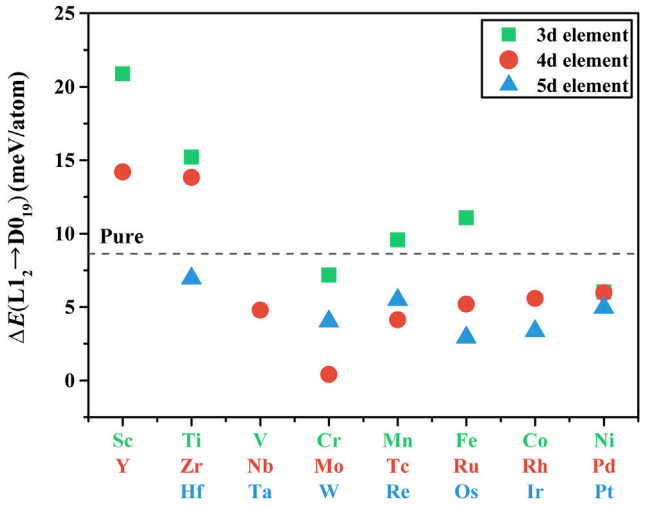

FIGURE 3 | Calculated structure transition energy of X-substituted γ′-Co_3(V, Ta), where 3d-, 4d-, and 5d-elements are denoted by square, round, and triangle, respectively.

3 RESULTS AND DISCUSSION

3.1 Site Preference and Phase Stability

The reaction energy $E_{sub}^{X \rightarrow i}$ of TM elements is plotted in **Figure 2**. The more negative the value of $E_{sub}^{X \rightarrow i}$, the stronger is the tendency for X to occupy this site. As seen, TM elements on the left side of the periodic table (Sc, Ti, Y, Zr, Nb, Mo, Hf, and W) tend to occupy V sites, whereas elements on the right side (Cr, Mn, Fe, Ni, Tc, Ru, Rh, Pd, Re, Os, Ir, and Pt) prefer the Co site. The results indicate that substitutional sites are closely related to the atomic radius. For TM elements with a large radius, V sites are preferred because the V atom is larger than the Co atom. For TM elements with a smaller radius, Co sites are preferred. The high reaction energy of TM elements at Ta sites indicates that no TM elements occupy Ta sites.

The formation enthalpies ΔH are tabulated in **Table 1**. Here, the TM elements at their most preferred substitutional sites were considered. Without considering the competing phase like $D0_{19}$, a negative value of ΔH indicates that this phase is thermodynamically allowed. It can be seen that ΔH for all TM-substituted γ′-Co_3(V, Ta) phases are negative, suggesting they are stable or metastable at 0 K.

Other than ΔH, the stability of the $L1_2$ structure is also related to the formation enthalpy of the competitive phase in the Co-based superalloys. The phase transfer energy $\Delta E(L1_2 \rightarrow D0_{19})$ is illustrated in **Figure 3**. $\Delta E(L1_2 \rightarrow D0_{19})$ is an indicator of the relative stability between the $L1_2$ and $D0_{19}$ structure. A negative value indicates that the $D0_{19}$ phase is more stable than the $L1_2$ phase at 0K and vice versa.

3.2 Effect of TM Elements on Mechanical Properties

To investigate the alloying effects of TM elements on the mechanical properties, the elastic constants C_{ij}, bulk modulus B, shear modulus G, Young's modulus E, and Poisson's ratio ν were calculated, as shown in **Table 2**. The predicted B, G, and E of γ′-Co_3(V, Ta) of previous theoretical results (Ruan et al., 2020) are also listed to validate our results.

As seen, the elastic constants are remarkably changed by TM elements. We evaluated the mechanical stability of the TM-substituted γ′-Co_3(V, Ta) phase using the Born criterion

TABLE 2 | Elastic properties of γ′-Co_3(V, Ta), including elastic constants C_{ij}, bulk modulus B, shear modulus G, Young's modulus E, and Poisson's ratio ν. (C_{ij}, B, G, and E are given by GPa).

Compound	Source	C_{11}	C_{12}	C_{44}	B	G	E	B/G	ν
Pure	This work	380.1	183.0	185.5	249	144	362	1.73	0.257
	Cal. (Ruan et al., 2020)				250	143	360	1.75	
$Co_{24}V_5Ta_2Sc$	This work	351.1	177.6	175.9	235	132	335	1.78	0.263
$Co_{24}V_5Ta_2Ti$	This work	371.8	183.7	183.0	246	140	353	1.76	0.261
$Co_{23}V_6Ta_2Cr$	This work	369.5	184.6	177.0	246	136	345	1.81	0.267
$Co_{23}V_6Ta_2Mn$	This work	367.0	179.6	180.3	242	139	349	1.75	0.260
$Co_{23}V_6Ta_2Fe$	This work	373.9	183.6	181.9	247	140	354	1.76	0.261
$Co_{23}V_6Ta_2Ni$	This work	384.2	186.9	182.6	253	143	360	1.77	0.262
$Co_{24}V_5Ta_2Y$	This work	343.0	168.8	161.3	227	126	319	1.80	0.266
$Co_{24}V_5Ta_2Zr$	This work	359.7	178.1	174.0	239	134	339	1.78	0.263
$Co_{24}V_5Ta_2Nb$	This work	375.0	182.7	182.3	247	141	355	1.75	0.260
$Co_{24}V_5Ta_2Mo$	This work	388.9	185.2	185.4	253	146	367	1.74	0.258
$Co_{23}V_6Ta_2Tc$	This work	366.2	191.9	177.5	250	133	339	1.88	0.274
$Co_{23}V_6Ta_2Ru$	This work	372.7	187.4	184.7	249	140	354	1.78	0.264
$Co_{23}V_6Ta_2Rh$	This work	375.8	181.2	185.1	246	143	359	1.72	0.257
$Co_{23}V_6Ta_2Pd$	This work	374.8	179.0	181.7	244	142	356	1.72	0.257
$Co_{24}V_5Ta_2Hf$	This work	362.6	180.2	177.9	241	136	343	1.77	0.262
$Co_{24}V_5Ta_2W$	This work	387.1	180.8	187.0	250	147	369	1.69	0.253
$Co_{23}V_6Ta_2Re$	This work	373.6	190.6	178.4	252	136	346	1.85	0.271
$Co_{23}V_6Ta_2Os$	This work	371.3	190.4	183.6	251	138	350	1.82	0.267
$Co_{23}V_6Ta_2Ir$	This work	368.9	171.6	186.7	237	144	360	1.64	0.247
$Co_{23}V_6Ta_2Pt$	This work	381.4	175.2	184.5	244	146	365	1.67	0.250

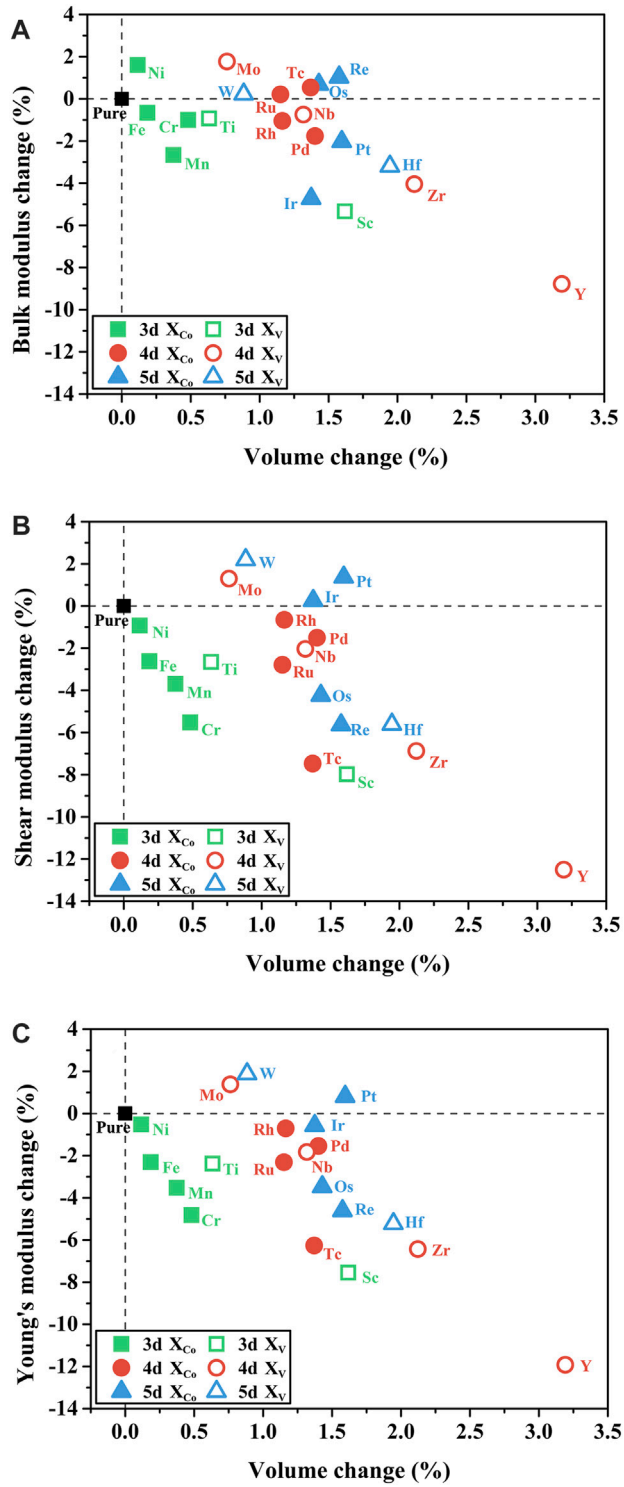

FIGURE 4 | Relationship between the elastic modulus changes and volume changes of X-substituted γ′-Co_3(V, Ta): **(A)** bulk modulus ***B***, **(B)** shear modulus ***G***, and **(C)** Young's modulus ***E***.

(Born, 1939): $C_{11} > 0$, $C_{44} > 0$, $C_{11} > |C_{12}|$, $C_{11} + 2C_{12} > 0$. It was confirmed that all TM-substituted γ′-Co_3(V, Ta) phases are mechanically stable.

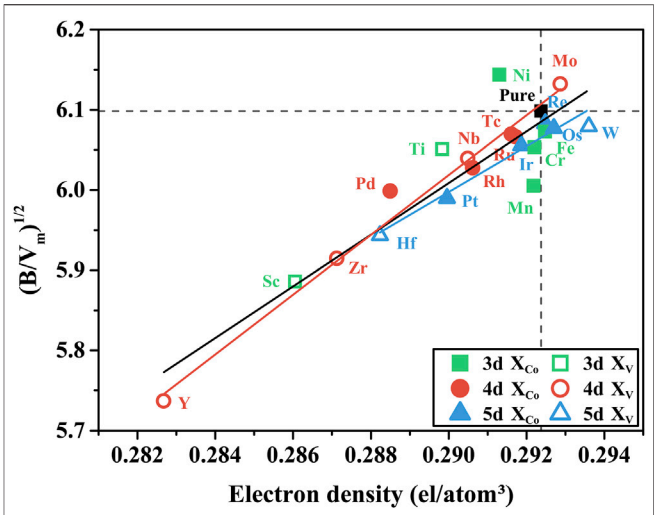

FIGURE 5 | Relationship between the electron density and $(B/V_m)^{1/2}$ of TM-substituted γ′-Co_3(V, Ta). The units of ***B*** and V_m are GPa and 10^{-6} m^3/mol, respectively.

To reveal the changing pattern of elastic properties induced by TM elements, the volume change concerning elastic properties is plotted in **Figure 4**. The doped TM elements cause the volume to expand despite the different substitutional sites (Co and Ta), which can be explained by a larger atomic radius of TM elements than that of their substituted atom. For 3d and 4d elements, the bulk/shear modulus change with respect to the volume change exhibits negative correlation, namely, expansion in volume and reduction in the bulk/shear modulus. However, for 5d elements, this relationship no longer holds. It is believed that mechanical properties have a strong correlation with the electron density in pure metals and binary alloys (Miedema et al., 1973). **Figure 5** plots the relationship between the electron density $(B/V_m)^{1/2}$, where the electron density n is defined by

$$n = Z_B / V_m, \tag{16}$$

where Z_B is the total valence electron number of X-doped Co_3(V, Ta), and V_m is the mole volume.

It can be seen that $(B/V_m)^{1/2}$ is proportional to the electron density for 4d- and 5d-elements. However, for 3d elements, this relationship breaks down. Hence, we concluded that both the volume change and electron density affect the elastic modulus, whereas for 3d elements, the volume change is the key factor. For 5d elements, the electron density becomes the key factor. For 4d elements, these two factors have comparable influences.

To further investigate the mechanism that how TM elements affect the elastic modulus of the γ′-Co_3(V, Ta) phase, their charge density difference (CDD) on the (100) plane is plotted in **Figure 6**. Here, we selected two elements W and Y that significantly changed the shear modulus ***G*** (the ***G*** of the γ′-Co_3(V, Ta) phase is raised from 144 to 147 when W is doped, and it is lowered to 126 when Y is doped). The CDD of pure γ′-Co_3(V, Ta) was also plotted for comparison. The distribution of interatomic valence electrons on the (100) plane can be judged

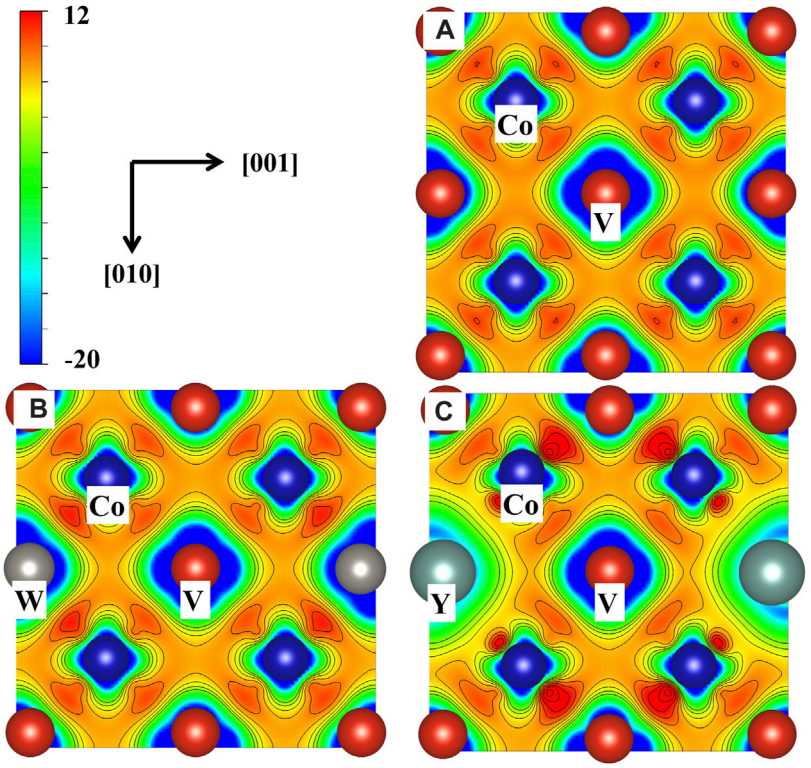

FIGURE 6 | Charge density differences (CDD) of the γ′-Co_3(V, Ta) phase on the (100) plane of **(A)** pure, **(B)** W occupying the V site, and **(C)** Y occupying the V site.

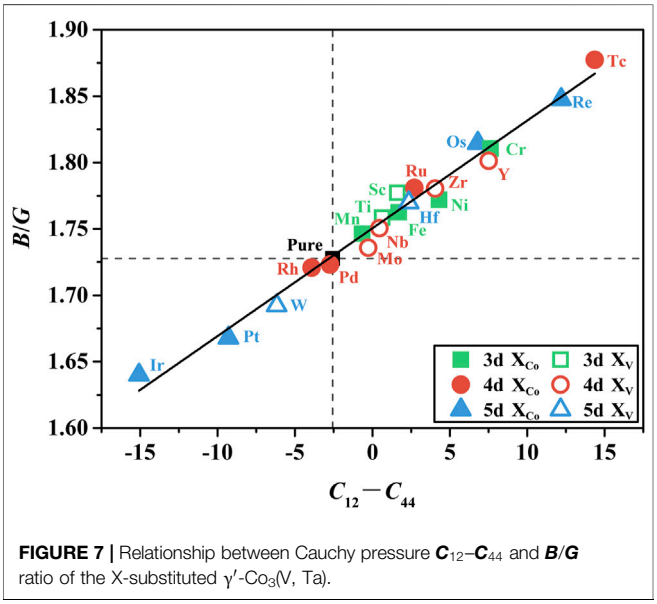

FIGURE 7 | Relationship between Cauchy pressure C_{12}–C_{44} and *B*/*G* ratio of the X-substituted γ′-Co_3(V, Ta).

by the shades of colors, and the darker the color, the more concentrated the valence electrons are, and the stronger the corresponding bonds are. As shown in **Figure 6A**, the valence electrons of the pure γ′-Co_3(V, Ta) phase on the (100) plane are mainly concentrated between the Co and V atoms, forming a very obvious covalent interaction. The doping of W does not significantly change the shape of the charge distribution but slightly increases the charge density between the W and the nearest neighboring Co atom, which means that the strength of the newly formed Co–W bond is greater than that of the original Co–V, resulting in a small increase of the shear modulus. Y, however, drastically changes the charge distribution on the (100) plane. Since Y has a much larger atomic radius than V, its doping causes significant lattice expansion in the γ′-Co_3(V, Ta) phase, resulting in Y crowding out the Co atoms and concentrating the charge between Co and V on the Y and Co lines, as shown in **Figure 6C**. The strength of the Co–V bond along the Y–Co direction is much stronger than that without doping, and the charge density around the Y atom is significantly reduced. This asymmetric charge distribution makes the crystal structure less resistant to shear deformation.

The ductility of the γ′-Co_3(V, Ta) phase after doping with TM elements was further evaluated using the Pugh's classical criterion and Cauchy pressure. According to Pugh's theory (Pugh, 1954), the value of B/G represents the ductility of materials. The critical value to distinguish the material ductility from brittleness is 1.75, and the higher the ratio, the more tough the material is, and conversely, the lower the ratio, the more brittle the material tends to be. On the other hand, Pettifor (1992) suggested that the Cauchy pressure (C_{12}–C_{44}) is a sign of atomic bonding within crystals, and systems with positive values of Cauchy pressure are dominated by metallic bonds, while systems with negative values

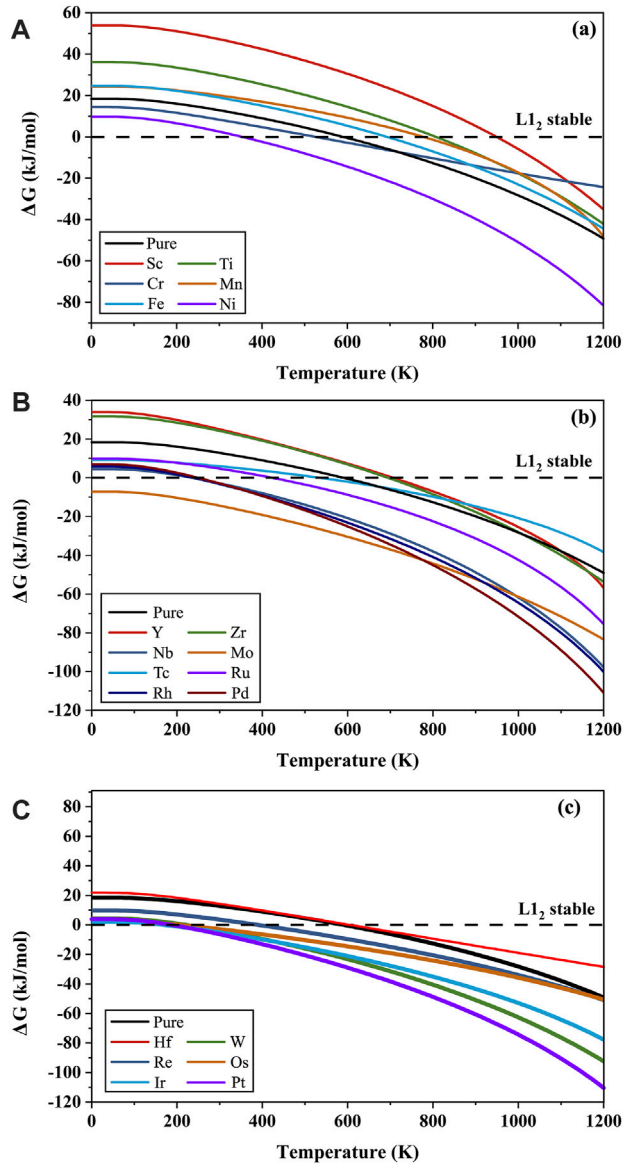

FIGURE 8 | Gibbs free energy difference ΔG of $L1_2$-Co_3(V, Ta) and $D0_{19}$-Co_3(V, Ta) doped with: **(A)** 3d elements, **(B)** 4d elements, and **(C)** 5d elements.

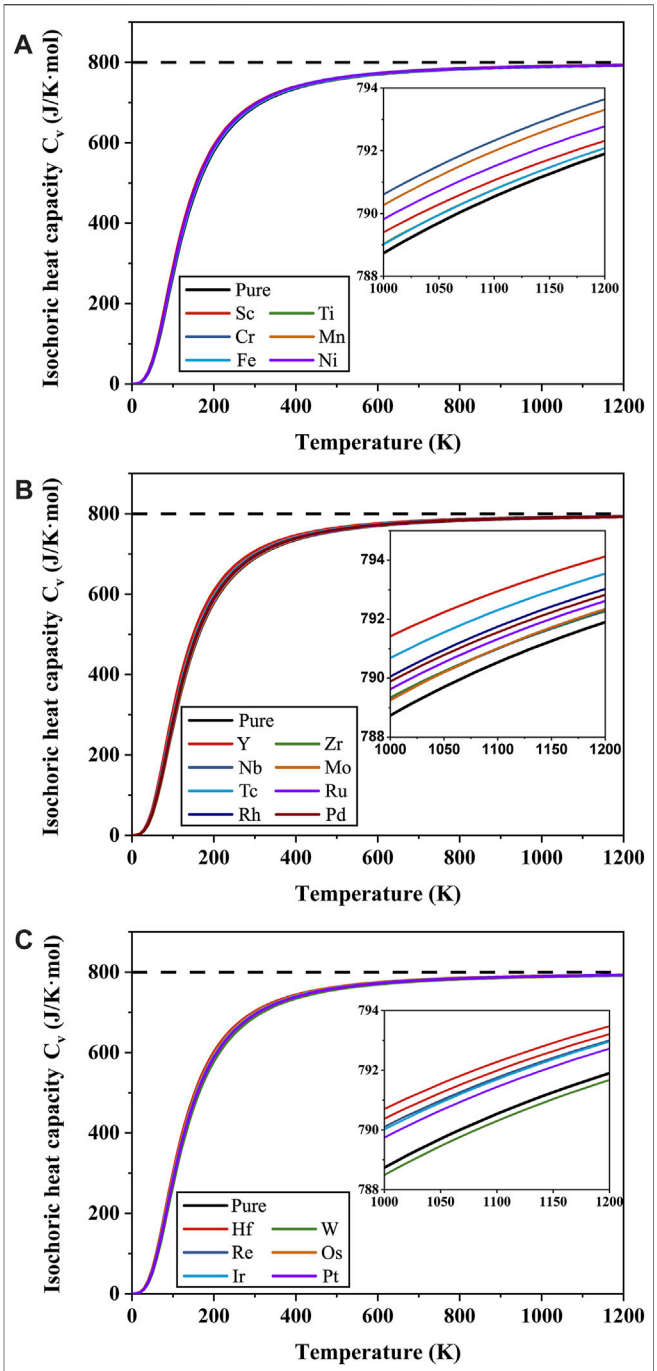

FIGURE 9 | Isochoric heat capacity C_v of γ′-Co_3(V, Ta) doped with **(A)** 3d elements, **(B)** 4d elements, and **(C)** 5d elements.

are dominated by covalent bonds. For metallic systems, higher Cauchy pressure means that the system is more ductile. To clarify the intrinsic relationship between atomic bonding and ductility, **Figure 7** plots the B/G value versus the Cauchy pressure. It is clear that there is a linear relationship between the B/G value and the Cauchy pressure, which indicates that the ductility of the γ′-Co_3(V, Ta) phase doped with X is mainly due to the influence of the metallic bonding within the structure. As shown in **Figure 7**, the undoped γ′-Co_3(V, Ta) phase exhibits intrinsic brittleness, and doping of TM elements changes the ductility of the γ′-Co_3(V, Ta) phase, for example, the addition of Tc, Re, and Os increases the Corsi pressure of the γ′-Co_3(V, Ta) phase, which enhances its internal metallicity and thus significantly improves the ductility of the γ′-Co_3(V, Ta) phase, which means that these elements can improve the mechanical properties of the γ′-Co_3(V, Ta) phase. In contrast, doping of Ir, Pt, W, Rh, and Pd causes the brittleness of the γ′-Co_3(V, Ta) phase, which reduces the mechanical properties.

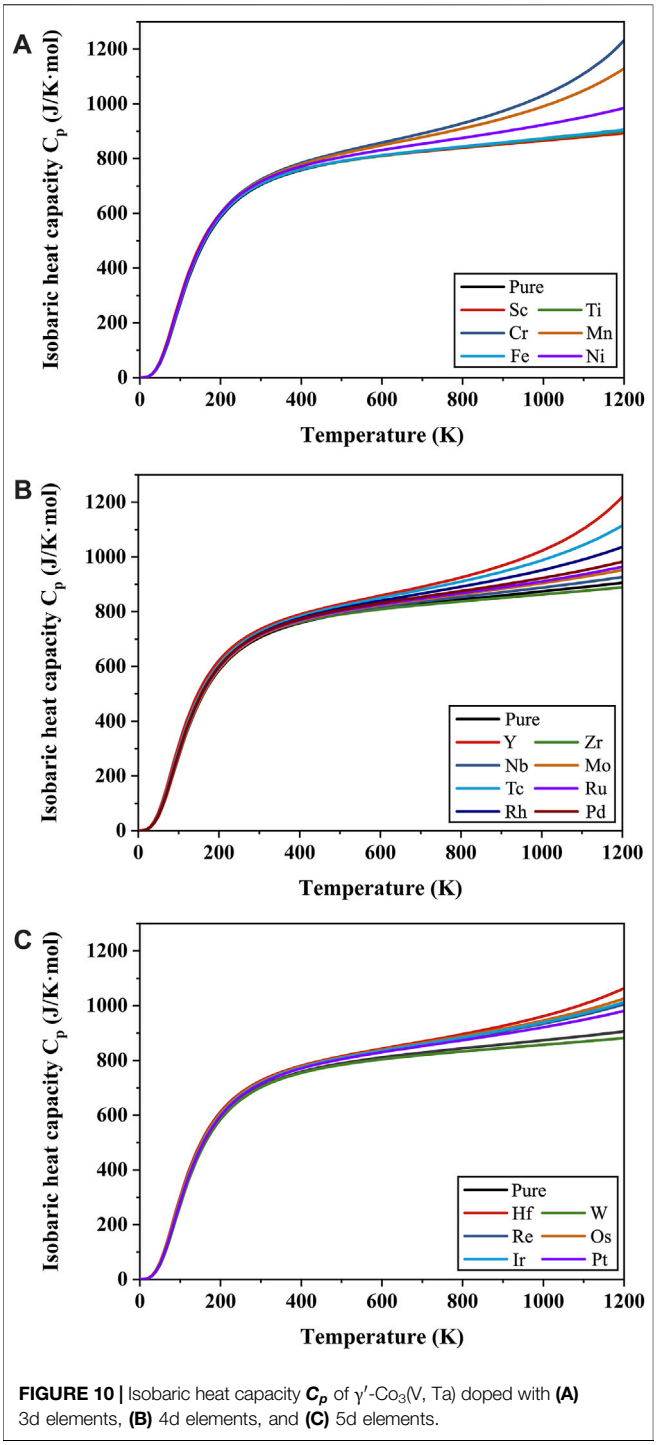

FIGURE 10 | Isobaric heat capacity C_p of γ′-Co_3(V, Ta) doped with **(A)** 3d elements, **(B)** 4d elements, and **(C)** 5d elements.

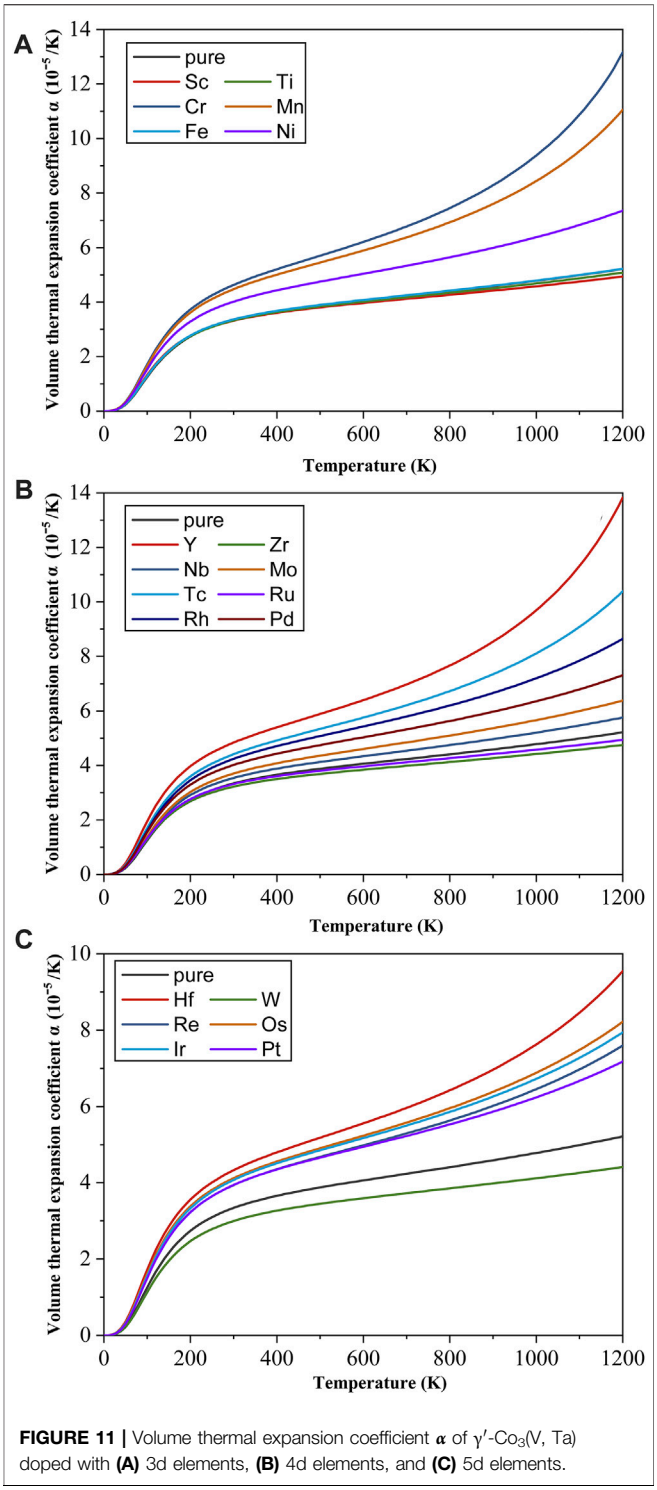

FIGURE 11 | Volume thermal expansion coefficient α of γ′-Co_3(V, Ta) doped with **(A)** 3d elements, **(B)** 4d elements, and **(C)** 5d elements.

3.3 Effect of TM Elements on the Thermodynamic Properties of the γ′-Co_3(V, Ta) Phase

Based on the Debye model of quasi-harmonic approximation (Francisco et al., 2001; Blanco et al., 2004), we investigated the thermodynamic properties of the γ′-Co_3(V, Ta) phase at elevated temperature using the Gibbs2 program (Otero-de-la-Roza et al., 2011). First, we discussed the relative stability of the γ′-Co_3(V, Ta) phase by analyzing the Gibbs free energy difference between the $L1_2$ structure and the $D0_{19}$ structure. The definition of the Gibbs free energy difference is as follows:

$$\Delta G = G_{D0_{19}} - G_{L1_2}, \tag{18}$$

where $G_{D0_{19}}$ and G_{L1_2} are the Gibbs free energy of $D0_{19}$ and $L1_2$ structures, respectively. When $\Delta G > 0$, it means that the $L1_2$ structure is more stable than the $D0_{19}$ structure and vice versa. **Figure 8** plots ΔG at 0–1200 K as a function of temperature. It can be seen that phonon contribution helps stabilize the $D0_{19}$ structure at elevated temperature. When no TM elements are doped, the Gibbs free energy of $D0_{19}$-Co_3(V, Ta) is lower than that of $L1_2$-Co_3(V, Ta) from about 600 to 1200 K, indicating that $L1_2$-Co_3(V, Ta) is unstable at high temperature. By comparing the doped and undoped ΔG, the effects of TM elements on the relative stability of the γ′-Co_3(V, Ta) phase at finite temperature can be divided into the following three categories:

1) Sc, Ti, Mn, Fe, and Hf can improve the relative stability of the γ′-Co_3(V, Ta) phase in the entire temperature range of 0–1200 K. The calculated results are compared with experimental results. According to Ruan et al. (2020), the γ′ phase decomposition was observed in the Co–12V–2Ta alloy that annealed at 800°C for 720 hours. When doped with Ti, the γ′ phase is maintained under the same anneal condition, which is in good agreement with the prediction in this study.
2) Elements that increase the relative stability of the γ′-Co_3(V, Ta) phase in some temperature ranges, namely, Cr, Y, Zr, and Tc. Although the doping of Cr and Tc will reduce the relative stability of the γ′-Co_3(V, Ta) phase at low temperatures, the relative stability of the γ′-Co_3(V, Ta) phase will increase as the temperature rises from about 700 K.
3) Ni, Nb, Mo, Ru, Rh, Pd, W, Re, Os, Ir, and Pt reduced the relative stability of the γ′-Co_3(V, Ta) phase in the entire temperature range of 0–1200 K. Among them, the doping of the TM Mo will make it negative in the entire temperature range, which means that the Mo-doped $L1_2$-Co_3(V, Ta) is always in a metastable state. Ruan et al. (2020) showed that the decomposition of the γ′ phase is observed after annealing at 800°C for 48 hours in the Co–12V–2Ta alloy doped with Nb, Ni, Mo, and W, which agrees well with our calculation results.

Then, the change of isochoric heat capacity C_v with temperature is discussed as it is an important thermodynamic quantity. As shown in **Figure 9**, the curve shows the typical characteristics of the isochoric heat capacity, that is, it follows the Debye model ($C_v(T) \propto T^3$) at low temperatures and approaches 800 J/K·mol at high temperatures, which is the Dulong–Petit limit ($C_v = 3nR$) [39]. The C_v of γ′-Co_3(V, Ta) phases after doping with different TM elements is not much different except for W. When W is doped, the C_v of the γ′-Co_3(V, Ta) phase is reduced, while other doping elements increase the C_v. **Figure 10** shows the change of γ′-Co_3(V, Ta) isobaric heat capacity C_p with temperature. The C_p is greater than C_v in the entire temperature range and satisfies the relationship $C_p - C_v = \alpha BVT$ (α is the bulk thermal expansion coefficient, and B is the bulk modulus). At low temperatures, C_p exhibits the same Debye model law as C_v, and then, C_p increases monotonously with increasing temperature which deviates from C_v, exceeding the Dulong–Petit limit (Kittel and Hellwarth, 1957). This difference in heat capacity is mainly caused by the non-simple harmonic effect caused by thermal expansion. When doped with Cr, Mn, Y, Tc, Rh, and Hf, the C_p curve at high temperature will be much higher than that of pure γ′-Co_3(V, Ta), which means that doping these elements will increase the sensitivity C_p to temperature. When Ti and Fe are doped, C_p basically remains unchanged. When elements such as Sc, Zr, and W are doped, the isobaric heat capacity of the γ′ phase will be slightly reduced.

Finally, the effect of TM elements on the volume thermal expansion coefficient α of the γ′-Co_3(V, Ta) phase at a finite temperature is calculated, and the results are shown in **Figure 11**. The α of the γ′-Co_3(V, Ta) phase after doping exhibits the same pattern at low temperature, that is, it increases sharply within 200 K, and then, the growth rate gradually slows down. The difference is that the doping of Sc, Ti, Fe, Zr, Ru, W, and other elements makes the volume thermal expansion coefficient of the γ′-Co_3(V, Ta) phase tends to be a constant at high temperature, indicating that its dependency on temperature is low. Other TM elements will significantly increase the volume thermal expansion coefficient at high temperature, especially Cr, Mn, Y, Tc, Rh, and Hf. When the temperature is greater than 1000 K, the volume thermal expansion coefficient rises exponentially with the temperature, indicating that the doping of these elements will cause the γ′-Co_3(V, Ta) phase to undergo a large volume change with the increase in temperature at high temperatures, thereby reducing its mechanical properties.

4 CONCLUSION

In this study, the first-principle–based density function theory (DFT) is used to investigate the effect of TM elements X (X = Sc, Ti, Cr, Mn, Fe, Ni, Y, Zr, Nb, Mo, Tc, Ru, Rh, Pd, Hf, W, Re, Os, Ir, and Pt) on the structural stability, mechanical properties, and thermodynamic properties of the γ′-Co_3(V, Ta) phase. The main results are as follows:

(1) The occupancy tendency of TM elements in the γ′-Co_3(V, Ta) phase was obtained by comparing the substitutional reaction energies of each non-equivalent site in the ground state: Sc, Ti, Y, Zr, Nb, Mo, Hf, and W atoms occupied the V atomic site; Cr, Mn, Fe, Ni, Tc, Ru, Rh, Pd, Re, Os, Ir, and Pt atoms occupied the Co atomic site. The structural transition energy showed that X-doped Co_3(V, Ta) phases are all more stable in the $L1_2$ structure than that the in $D0_{10}$ structure in the ground state, and some of the TM elements can enhance the relative stability of the γ′ phase, such as Sc, Ti, Y, Zr, Fe, and Mn.
(2) In the ground state, the γ′-Co_3(V, Ta) phases are all mechanically stable after the doping of TM elements. The addition of Mo and W increases the bulk modulus, shear modulus, and Young's modulus. When doped with 3d elements, the volume change is an important factor affecting its elastic modulus. When doped with 4d elements, the volume change and electron density affect its

elastic modulus simultaneously. When doped with 5d elements, the effect of electron density on its elastic modulus is more important than the volume change. According to Pugh's classical criterion, the γ′-Co_3(V, Ta) phase is an intrinsically brittle material, and the addition of elements such as Tc and Re can significantly enhance the ductility.

(3) The $L1_2$ structure of Co_3(V, Ta) is more stable than the $D0_{19}$ structure in the temperature range from 0 to 600 K, and the $D0_{19}$ structure is more stable in the temperature range from 600 to 1200 K. The doping of Sc, Ti, Mn, Fe, and Hf enhances the relative stability of the γ′-Co_3(V, Ta) phase in the whole temperature range from 0 to 1200 K. The doping of TM elements does not significantly change the isovolumetric heat capacity $\boldsymbol{C_v}$. The isobaric heat capacity $\boldsymbol{C_p}$ and the bulk thermal expansion coefficient $\boldsymbol{\alpha}$ of the γ′-Co_3(V, Ta) phase doped with Cr, Mn, Y, Tc, Rh, and Hf elements increased significantly with the temperature at elevated temperature, while the doping of Sc, Ti, Fe, Zr, Ru, and W elements does not significantly change the isobaric heat capacity $\boldsymbol{C_p}$ and bulk thermal expansion coefficient $\boldsymbol{\alpha}$.

DATA AVAILABILITY STATEMENT

The raw data supporting the conclusion of this article will be made available by the authors, without undue reservation.

AUTHOR CONTRIBUTIONS

Conceptualization: XL and CW. Formal analysis: YC and JH. Investigation: YC, CZ, and CY. Original draft preparation: YC and JH. Writing—review and editing: YC and JH. Visualization: YC and JH. Supervision: XL and CW.

FUNDING

This work was supported by the Key-Area Research and Development Program of Guangdong Province (No. 2019B010943001) and the National Natural Science Foundation of China (Grant No. 51831007).

REFERENCES

Bantounas, I., Gwalani, B., Alam, T., Banerjee, R., and Dye, D. (2019). Elemental Partitioning, Mechanical and Oxidation Behaviour of Two High-γ′ W-free γ/γ′ Polycrystalline Co/Ni Superalloys. *Scr. Mater.* 163, 44–50. doi:10.1016/j.scriptamat.2018.12.025

Blanco, M. A., Francisco, E., and Luaña, V. (2004). GIBBS: Isothermal-Isobaric Thermodynamics of Solids from Energy Curves Using a Quasi-Harmonic Debye Model. *Comput. Phys. Commun.* 158 (1), 57–72. doi:10.1016/j.comphy.2003.12.001

Born, M. (1939). Thermodynamics of Crystals and Melting. *J. Chem. Phys.* 7 (8), 591–603. doi:10.1063/1.1750497

Davydov, D., Kazantseva, N., Ezhov, I., and Popova, E. (2021). Effect of Alloying on the γ-γ′ Microstructure of W-free Co-based Superalloys. *Mater. Today Proc.* 38, 1971–1973. doi:10.1016/j.matpr.2020.09.131

Drapier, J. M., and Coutsouradis, D. (1968). Precipitation Hardening of Co-Cr-Ta Alloys. *Cobalt* 39, 63–74.

Francisco, E., Blanco, M. A., and Sanjurjo, G. (2001). Atomistic Simulation of SrF_2 Polymorphs. *Phys. Rev. B* 63 (9), 094107. doi:10.1103/physrevb.63.094107

Kittel, C., and Hellwarth, R. W. (1957). Introduction to Solid State Physics. *Phys. Today* 10 (6), 43–44. doi:10.1063/1.3060399

Kresse, G., and Furthmüller, J. (1996). Efficient Iterative Schemes Forab Initiototal-Energy Calculations Using a Plane-Wave Basis Set. *Phys. Rev. B* 54 (16), 11169–11186. doi:10.1103/physrevb.54.11169

Kresse, G., and Joubert, D. (1999). From Ultrasoft Pseudopotentials to the Projector Augmented-Wave Method. *Phys. Rev. B* 59 (3), 1758–1775. doi:10.1103/physrevb.59.1758

Methfessel, M., and Paxton, A. T. (1989). High-precision Sampling for Brillouin-Zone Integration in Metals. *Phys. Rev. B* 40 (6), 3616–3621. doi:10.1103/physrevb.40.3616

Miedema, A. R., Boer, F. R. d., and Chatel, P. F. d. (1973). Empirical Description of the Role of Electronegativity in Alloy Formation. *J. Phys. F. Metall. Phys.* 3 (8), 1558–1576. doi:10.1088/0305-4608/3/8/012

Migas, D., Moskal, G., and Maciąg, T. (2020). Thermal Analysis of W-free Co-(Ni)-al-mo-nb Superalloys. *J. Therm. Anal. Calorim.* 142 (1), 149–156. doi:10.1007/s10973-020-09375-7

Monkhorst, H. J., and Pack, J. D. (1976). Special Points for Brillouin-Zone Integrations. *Phys. Rev. B* 13 (12), 5188–5192. doi:10.1103/physrevb.13.5188

Otero-de-la-Roza, A., Abbasi-Pérez, D., and Luaña, V. (2011). Gibbs2: A New Version of the Quasiharmonic Model Code. II. Models for Solid-State Thermodynamics, Features and Implementation. *Comput. Phys. Commun.* 182 (10), 2232–2248. doi:10.1016/j.cpc.2011.05.009

Pettifor, D. G. (1992). Theoretical Predictions of Structure and Related Properties of Intermetallics. *Mater. Sci. Technol.* 8 (4), 345–349. doi:10.1179/mst.1992.8.4.345

Pollock, T. M., Dibbern, J., Tsunekane, M., Zhu, J., and Suzuki, A. (2010). New Co-based γ-γ′ High-Temperature Alloys. *JOM* 62 (1), 58–63. doi:10.1007/s11837-010-0013-y

Pugh, S. F. (1954). XCII. Relations between the Elastic Moduli and the Plastic Properties of Polycrystalline Pure Metals. *Lond. Edinb. Dublin Philosophical Mag. J. Sci.* 45 (367), 823–843. doi:10.1080/14786440808520496

Pyczak, F., Bauer, A., Göken, M., Lorenz, U., Neumeier, S., Oehring, M., et al. (2015). The Effect of Tungsten Content on the Properties of L12-Hardened Co–al–W. *J. Alloys Compd.* 632, 110–115. doi:10.1016/j.jallcom.2015.01.031

Reyes Tirado, F. L., Taylor, S., and Dunand, D. C. (2019). Effect of Al, Ti and Cr Additions on the γ-γ' Microstructure of W-free Co-ta-V-based Superalloys. *Acta Mater.* 172, 44–54. doi:10.1016/j.actamat.2019.04.031

Reyes Tirado, F. L., Taylor, S. V., and Dunand, D. C. (2020). Low-density, W-free Co-nb-V-al-based Superalloys with γ/γ' Microstructure. *Mater. Sci. Eng. A* 796, 139977. doi:10.1016/j.msea.2020.139977

Ruan, J., Xu, W., Yang, T., Yu, J., Yang, S., Luan, J., et al. (2020). Accelerated Design of Novel W-free High-Strength Co-base Superalloys with Extremely Wide γ/γ′ Region by Machine Learning and CALPHAD Methods. *Acta Mater.* 186, 425–433. doi:10.1016/j.actamat.2020.01.004

Sato, J., Omori, T., Oikawa, K., Ohnuma, I., Kainuma, R., and Ishida, K. (2006). Cobalt-Base High-Temperature Alloys. *Science* 312 (5770), 90–91. doi:10.1126/science.1121738

Shang, S., Wang, Y., and Liu, Z.-K. (2007). First-principles Elastic Constants of α- and θ-Al2O3. *Appl. Phys. Lett.* 90 (10), 101909. doi:10.1063/1.2711762

Shi, L., Yu, J. J., Cui, C. Y., and Sun, X. F. (2015). Microstructural Stability and Tensile Properties of a Ti-Containing Single-Crystal Co-ni-al-W-base Alloy. *Mater. Sci. Eng. A* 646, 45–51. doi:10.1016/j.msea.2015.08.044

Wang, C. P., Deng., B., Xu., W. W., Yan., L. H., Han., J. J., and Liu., X. J. (2018). Effects of Alloying Elements on Relative Phase Stability and Elastic Properties of L12 Co3V from First-Principles Calculations. *J. Mater Sci.* 53 (2), 1204–1216. doi:10.1007/s10853-017-1549-9

Conflict of Interest: The authors declare that the research was conducted in the absence of any commercial or financial relationships that could be construed as a potential conflict of interest.

Publisher's Note: All claims expressed in this article are solely those of the authors and do not necessarily represent those of their affiliated organizations, or those of the publisher, the editors and the reviewers. Any product that may be evaluated in this article, or claim that may be made by its manufacturer, is not guaranteed or endorsed by the publisher.